INORGANIC CHEMISTRY

FRONTIERS

Accepted Manuscript

INORGANIC CHEMISTRY

FRONTIERS

http://rsc.li/frontiers-inorganic

Chinese Chemical Society
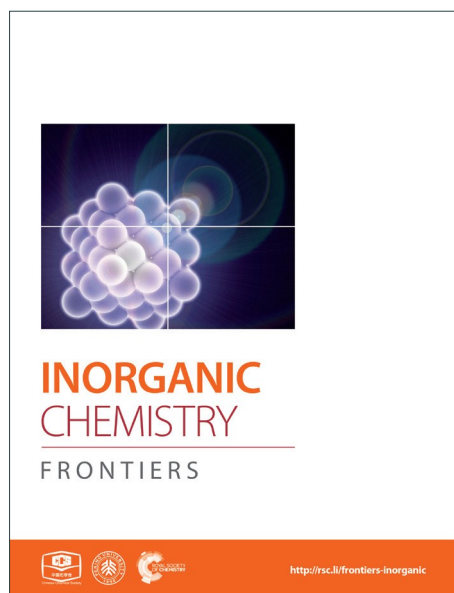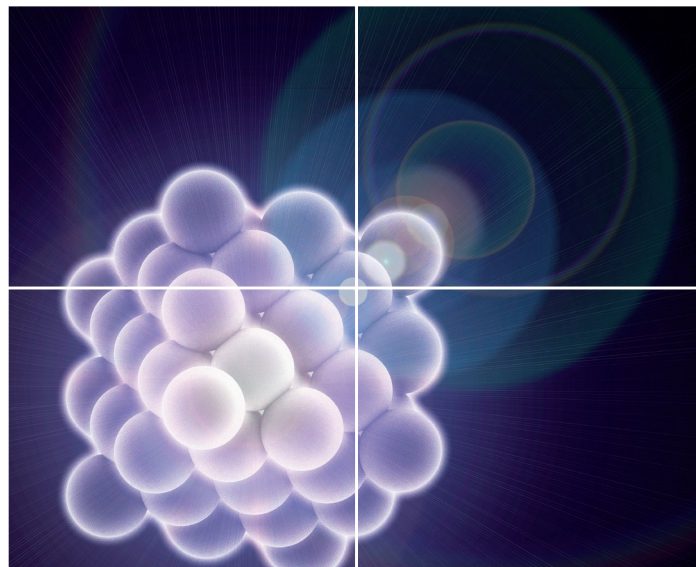
ROYAL SOCIETY OF CHEMISTRY

http://rsc.li/frontiers-inorganic

Journal Name

Dynamic Article Links ▶

ARTICLE TYPE

Cerium-based porous coordination polymer with hierarchical superstructures: Fabrication, formation mechanism and its thermal conversion to hierarchical CeO$_2$

Yong-Xia Zhao, Zhi-Wen Nie, Meng-Meng Shi, Cheng-Hui Zeng, Yuan Li, Lei Wang*, Sheng-Liang Zhong*

In this work, cerium-based porous coordination polymer (Ce-CP) with hierarchical superstructures have been successfully synthesized on a large scale employing cerium nitrate as metal salt and 2,5-pyridinedicarboxylic acid (2,5-H$_2$pdc) as ligand by a mixed-solvothermal route. The as-obtained products were characterized by scanning electron microscopy (SEM), Fourier transform infrared spectroscopy (FTIR), X-ray powder diffraction (XRD), X-ray photoelectron spectra (XPS), thermogravimetry and differential thermal analysis (TG-DTA). It was found that the hierarchical superstructures are composed of asymmetric branches with lengths range from 10 to 50 μm. The reaction parameters such as reaction temperature, total concentrations of the reactants, solvent composition, and the reaction time were investigated systematically. A possible formation mechanism for the hierarchical superstructures has been proposed to interpret the growth process. CeO$_2$ with similar hierarchical structures could be obtained after thermolysis of the Ce-CP precursors at 450 $^{\circ}$C for 4 h. The UV-vis adsorption spectrum of the obtained CeO$_2$ shows that band gap energy (Eg) is 2.64 eV, which is lower than that of bulk ceria. Moreover, the as-obtained CeO$_2$ also exhibited remarkable ability to remove rhodamine B (RhB).

Introduction

Coordination polymer (CP) as a class of captivating inorganic-organic hybrid materials have received a great deal of attention because of their unique and high degree of tailorability, which have great potential technological applications in heterogeneous catalysis,[1] gas storage,[2] medicine imaging,[3] biosensing and drug delivery.[4] Up to now, with the on-going development of modern nanoscience and nanotechnology, a large number of CP with a wide variety of morphologies and structures have been synthesized successfully. For example, Wang et al. prepared hollow iron-based ferrocenyl CP microspheres with microporous shells via a one-pot solvothermal method without any additional template and discussed the Ostwald ripening mechanism of the microspheres.[5] Oh et al. also described a simple solvothermal approach for the synthesis of hexagonal-tube CP.[6] We have been engaged in the synthesis of CP micro/nanostructured materials during the past years.[7] All the previous work suggested that suitable selection of the metal ions, building organic ligands and design of reaction routes would not only enrich its family but also bring us some unexpected results on morphology control or fascinating properties.[8]

The hierarchical self-assembly micro/nanostructured materials built from functional low dimensional nanostructures have aroused extensive research interest owing to their enhanced properties and potential applications over the past decades.[9] The chemical and physical properties of solid-state materials depend not only on their size, shape, chemical composition, but their assemblies as well.[10] Thus, control over size and shape of hierarchical micro/nanostructures is an important theme for understanding and exploiting their unique properties.[9c] On the nanoscale, dendritic hyperbranched structures are formed by hierarchical self-assembly under non-equilibrium conditions.[11] Inspired by these results, many types of three dimensional (3D) micro/nanostructures with high complexity have been fabricated successfully, such as snowflakers,[12] nanocages,[13] hyperbranches,[14] multipods,[15] dendrites,[16] saws,[17] flower-like microspheres,[18] hollow nanospheres,[19] airplane-like nanostructures,[20] and so on. However, these structures mainly focus on metal, metal oxides, and other semiconductors. Until now, there are only sporadic successful examples of the synthesis of uniform hierarchical CP with rich morphologies.[21] Therefore, it still remains a significant challenge to design and develop an effectively and reliable route for synthesis CP hierarchical superstructures, regarding control over the complex structures.

Ceria is one of the most attractive rare-earth oxides, which have aroused extensive attention because of their candidate applications range from catalysis,[22] fuel cells,[23] sensors,[24] and UV blocking,[25] and so forth. The morphologies and structures of

College of Chemistry and Chemical Engineering, Jiangxi Normal University, Nanchang 330022, P. R. China.
E-mail: slzhong@jxnu.edu.cn (S. L. Zhong). Tel.:86-0791-88120386; fax: 86-0791-88120386.
† Electronic supplementary information (ESI) available: additional graphs, See DOI: 10.1039/c0000000x.

CeO_2 have important influence on their properties, the main emphasis on the CeO_2 has focused on the fabrication of various morphologies and structures.[26] So far, CeO_2 with various basic nanoscale morphologies and structures have been synthesized successfully through various of methods, such as nanoparticles,[27] nanowires,[28] nanotubes,[29] nanorods,[30] and so on. Furthermore, it has been demonstrated that 3D CeO_2 hierarchical structures display enhanced activity towards the removal of As(V) and Cr(VI) in wastewater.[31] In this respect, it is urgent to fabricate 3D hierarchical micro/nanostructured CeO_2 with various composites and morphologies based on different driving mechanisms, which endow them some unique properties and novel functionalities. Yang's group fabricated CeO_2 3D microflower structures via the calcination of a cerium oxalate precursor, and the as-prepared flowerlike CeO_2 displayed a high surface area (147.6 m^2 g^{-1}), which shows a higher catalytic activity for CO oxidation.[32] However, to the best of our knowledge, there have been very few reports focusing on CeO_2 3D hierarchical superstructures via the thermal treatment of the corresponding CP precursors.

In this work, building block 2,5-H_2pdc is chosen as a multidentate ligand to generate organic-inorganic hybrid materials, which is based on the following reasons: (i) 2,5-H_2pdc as an N-heterocyclic analog of 1,4-benzene-dicarboxylic (terephthalic) acid that combines the advantages of both organic multi-carboxylic acid and aromatic compounds.[33] (ii) the carboxylate groups of 2,5-H_2pdc can be completely or partially deprotonated to generate $pydc^{2-}$ and $Hpydc^-$, allowing various acidity-dependent coordination modes. (iii) 2,5-H_2pdc ligand possesses rich coordination modes due to different –O and –N donors (carboxylate oxygen atoms and pyridine nitrogen) that may be suitable to connect metal centers to generate metal-organic frameworks (MOFs) structures. In addition, our previous works have been proven that the 2,5-H_2pdc is an excellent building block for the construction of lanthanide coordination polymers.[7c,7f] Herein, we present a mixed-solvothermal route to fabricate a Ce-CP hierarchical superstructures from cerium(III) and well-known 2,5-H_2pdc building block. Influential factors including reaction time, temperature, total concentrations, and solvent composition of the reactants for the formation of the Ce-CP superstructures have been studied systematically. A possible formation mechanism of the Ce-CP hierarchical superstructures was suggested based on the detailed experiments. After thermal decomposition of the Ce-CP, CeO_2 with similar hierarchical structures were successfully fabricated.

Experimental section

Materials and synthesis

All the reagents used in our experiment were of analytical grade and used without further purification. In a typical synthesis procedure of the hierarchical superstructures (sample 1), 0.2 mmol of $Ce(NO_3)_3 \cdot 6H_2O$ was dissolved in 10 mL of absolute ethanol, followed by the addition of 22 mL of dmf (N,N-dimethylformaminde) containing 0.8 mmol of 2,5-pyridinedicarboxylic acid (2,5-H_2pdc). After vigorous stirring for 20 min under magnetic stirring, the resulting solution was transferred into a 40 mL teflon-lined autoclave and heated at 160 ^{o}C for 12 h. After the autoclave was cooled to room temperature

naturally, the fresh precipitates were collected by centrifugation, washed three times with absolute ethanol, and dried at 60 ^{o}C in vacuum. The detailed experimental conditions for the as-synthesized products are listed in Table S1 (ESI†). Finally, mesoporous CeO_2 was obtained by calcination of the Ce-CP precursor in air at 450 ^{o}C for 4 h with a heating rate of 0.5 ^{o}C min^{-1}.

Characterization

The phase and composition of the resulting products were analyzed by XRD, in a two theta range from 5° to 90°, using a Rigaku/Max-3A diffractometer. The morphologies and superstructures of the as-prepared products were examined by using SEM (HITACHI, S-3400N). Transmission electron microscopy (TEM), high-resolution TEM (HRTEM), and selected area electron diffraction (SAED) images were obtained by using a JEM 2100 transmission electron microscope operated at an accelerating voltage of 200 kV. Elemental analysis (EA) data were obtained using an EA 300 instrument. FTIR spectra were carried out on a Nicolet 6700 spectrometer in the wavenumbers ranging from 4000 cm^{-1} to 400 cm^{-1}. TG-DTA analysis was conducted with a TA-50 thermal analyzer instrument at a heating rate of 10 ^{o}C min^{-1} from room temperature to 1000 ^{o}C under an air atmosphere. Nitrogen adsorption–desorption isotherms were collected at liquid nitrogen temperature (77 K) using a BELSORP-mini II apparatus. The specific surface areas were calculated by (Brunauer–Emmett–Teller) BET methods, and the mesoproe size distribution was calculated from the adsorption branch using the Barrett–Joyner–Halenda (BJH) theory. The Raman spectra were recorded using a LabRAM HR laser Raman spectrometer with a 633 nm excitation. XPS were measured using an ESCALAB250 X-ray photoelectron spectrometer with Al Kα radiation. Ultraviolet-visible (UV-vis) adsorption spectrum was recorded on a SOLID3700 UV/VIS/NIR spectrophotometer. All the measurements were performed at room temperature.

Photocatalytic degradation experiments

Typical degradation experiments under high-pressure mercury lamp (500 W) were performed at room temperature. Prior to irradiation, 20 mL of RhB aqueous solution (5×10^{-6} M) containing 0.05 g CeO_2 were magnetically stirred for 30 min in dark continuously in order to achieve an adsorption/desorption equilibrium between the as-obtained CeO_2 and the RhB dye. Then the suspension was magnetically stirred under UV light irradiation. At regular intervals, aliquots of solution were withdrawn and centrifuged to separate solid particles for analysis of concentration. The characteristic absorbance of RhB at 554 nm was used to characterize the concentration of RhB. The photocatalytic reaction progress was monitored using a Lambda 35 UV-vis spectrometer.

Results and discussion

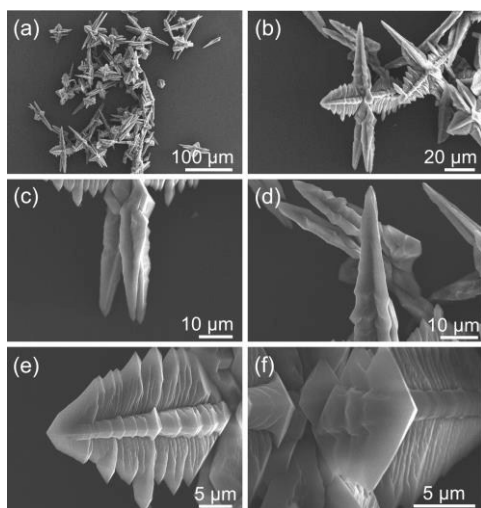### Characterization of the Ce-CP hierarchical superstructures

Fig. 1 SEM images of the Ce-CP hierarchical superstructures (sample 1).

The morphology, structures and size of the as-synthesized Ce-CP hierarchical superstructures were examined using SEM, as shown in Fig. 1. Fig. 1(a) is the low magnification SEM image, revealing that the Ce-CP hierarchical superstructures were synthesized on a large scale and in high purity after a mixed-solvothermal reaction. The magnified image of Fig. 1(b) indicates that the Ce-CP superstructures exhibit hierarchical structure. Each superstructure practically consisted of many branches attached to a mutual core. The length of the branches is in the range of 10-50 μm. A close observation on the vertical direction of a single superstructure, two or more taper-shape-like rods with lengths of about 30 μm could be observed in Fig. 1(c) and 1(d). Perpendicular to the taper-shape-like rods direction, it is found that there are four homogeneous dendritic structures with the lengths of the dendrite trunks are 10-25 μm, and a lot of sub-branches vertically distribute on the sides of the dendritic trunk (Fig. 1(e) and 1(f)). This asymmetric superstructure is not in the same plane but has a 3D superstructure, which is clearly different from the reported semiconductor superstructures.[34] Fig. S1(a)† shows the XRD pattern of Ce-CP hierarchical superstructures. It clearly displays that the peaks are strong and narrow, indicating the good crystallinity of the as-prepared products. However, it could not be finely indexed to a known phase compared with other references and all the standard XRD patterns in JCPDS cards. There are inherent difficulties in determining the exact crystalline information of Ce-CP through HRTEM, but it is reasonable to believe that such Ce-CP have been successfully prepared based on the above results.[35] Since CP micro/nanoparticles displayed unexplored crystalline structures, and the corresponding single crystals with a proper size could hardly be obtained, researchers have usually devoted to apply multi-analysis methods to study the compositions and structures of the CP micro/nanoparticles.[36]

Therefore, Ce-CP hierarchical superstructures were carefully characterized by XPS, FTIR, EA, and TG-DTA analysis to investigate their chemical structure and compositions. The XPS spectrum of the as-synthesized Ce-CP powder clearly detects the obvious peaks of cerium, carbon, nitrogen and oxygen in the survey spectrum (Fig. S1(b)†). From Fig. S1(c)†, four binding energy peaks in the 3d region at 881.18 eV, 884.38 eV, 900.18 eV, and 903.18 eV, in addition to the 4d region at 110.08 eV, which indicate that the oxidation state of cerium in these samples is from Ce(III). The FTIR spectrum of the CP superstructures (Fig. S1(d)†) displays different characteristics compared with pure 2,5-H_2pdc, which further confirms that the formation of Ce-CP hierarchical superstructures from the cerium ions and 2,5-H_2pdc. Firstly, the characteristic peaks at 1479 and 1417 cm^{-1} are attributed to the stretching vibrations of the backbone of the benzene ring.[37] Secondly, comparing with the absorption band at 1731 and 1385 cm^{-1} for the –COOH of free 2,5-H_2pdc ligand, the bands around 1607 and 1353 cm^{-1} could be assigned to the asymmetric vas(–COO^-) and symmetric vs(–COO^-) stretching vibrations of the ionized carboxylate groups, respectively.[38] Thirdly, the sharp band appears at 506 cm^{-1} is attributed to the Ce-O stretching vibration, which confirms that the Ce^{3+} ions are coordinated with the 2,5-H_2pdc to form a complex.[39] Elemental analysis (EA) analysis was performed to study the chemical compositions of the Ce-CP, providing the elemental quantities as follows: C: 36.18, N: 8.31, H: 3.23. Combining EA results and the building components determined by FTIR, the empirical formula of the Ce-CP could be proposed to Ce(pdc)(Hpdc)·2(dmf)·2(H_2O) (calcd C: 36.76, calcd N: 8.57, calcd H: 3.86%).[40] TG-DTA curves of Ce-CP taken in air (Fig. S1(e)†) further conducted to support our conjecture. There are three weight loss steps when the thermal decomposition of this compound. The first stage occurs before 184 ^oC, the weight loss is approximately 6.15%, corresponding to the weight of the physically absorbed and structured water molecules. The second weight loss in the range of 184-380 ^oC is 21.82%, which is related to the loss of dmf molecules.[41] The last weight loss from 380 to 445 ^oC is ascribed to the decomposition of organic ligand. N_2 adsorption-desorption isotherms were recorded after pretreatment at 150 ^oC for 4 h under dynamic vacuum. As shown in Fig. S1(f)†, N_2 adsorption isotherm of Ce-CP hierarchical superstructures exhibits the behaviour for multilayer adsorption. The BET surface areas of Ce-CP obtained from the adsorption branch of the isotherm gave a relatively low BET surface area of 2.22 m^2 g^{-1}. The low N_2 adsorption is more likely attributed to the strong quadrupole interactions between N_2 molecules and the electrostatic field gradients near the surface of Ce-CP hierarchical superstructures. These considerable quadrupole interactions could block N_2 molecules from passing into the pore channels.[42]

It is well known that the lanthanide elements are a group of 14 elements (except Pm, which is a radioactive element), which can be divided into light (La→Eu) and heavy (Gd→Lu) rare earth groups. Under identical synthetic conditions, other lanthanide-based CP were also prepared, just by replacing Ce^{3+} with other rare earth element ions.[7b] It is clearly observed from SEM images that the morphologies of the as-synthesized products are different to some extent (Fig. S2 and S3†). From La to Gd, similar CP hierarchical superstructures with the length of branches in range of 30-120 μm were prepared, while others lanthanide-based CP were close to spherical in shape with diameters of 5-20 μm and irregularly shaped microstructures with a random size distribution. Although the exact reason is not clear at present, it is reasonably believed that this difference seems to be closely related to the change of lanthanide ion radius.[43]

Influences of different reaction parameters on the morphologies of Ce-CP hierarchical superstructures

In order to better understand the formation mechanism of the Ce-CP hierarchical superstructures, a series of controlled experiments (Table S1, ESI†) were conducted to systematically study the morphology evolution.

By fixing other reaction conditions, the effect of the reaction temperature on the morphology of the as-prepared products were investigated. At the reaction temperature of 80 ^{o}C (sample 2), the products were composed of uniform nanospheres with a size of about 500 nm in diameter (Fig. S4(a)†). Interestingly, with the increase of reaction temperature, the hierarchical structures began to form. At 100 ^{o}C (sample 3), a large amount of approximate hierarchical cubes with edge lengths of about 30 μm were obtained (Fig. S4(b)†). Furthermore, hierarchical superstructures were also prepared with high yield at 140 ^{o}C (sample 4). Compared with the typical hierarchical superstructures mentioned above (sample 1), these hierarchical superstructures possess a narrow size distribution (Fig. S4(c)†). However, when the reaction was carried out at 180 ^{o}C (sample 5), hierarchical superstructures had been destroyed (Fig. S4(d)†). From these results, we can conclude that the Ce-CP hierarchical superstructures can be selectively synthesized by controlling the reaction temperature rationally. The high temperature is helpful for the formation of hierarchical superstructures, and the typical Ce-CP hierarchical superstructures can be achieved at 160 ^{o}C.

To determine the effect of total concentrations of the reactants on the formation of the products while keeping other reaction conditions the same, the images of the products obtained from the solutions with a mixed-solvothermal treatment at 160 ℃ for 12 h are shown in Fig. S5(a-c)†. It is obvious that the morphology changed greatly with increasing the amounts of reactants. When the Ce^{3+} was 0.05 mmol (sample 6) and the molar ratio of Ce^{3+} to 2,5-H_2pdc was 1:4 with other reaction conditions unchanged, uniform spheres with diameters of about 500 nm were obtained (Fig. S5(a)†) on a large scale, which was much different from the typical sample. To investigate whether hierarchical superstructures can be obtained by increasing the reaction time, experiment was carried out at 96 h (sample 7). However, no hierarchical superstructures were obtained. Instead, a large amount of octahedrons with a size distribution of about 27 μm in diameter were observed and a small amount of nanoparticles with diameters of *ca.* 100-350 nm were also detected (inset in Fig. S5(a)†). While increasing the amount of Ce^{3+} to 0.1 mmol (sample 8), the as-synthesized product mainly takes on mixed morphologies of nanoparticles and complicated hierarchical superstructures (Fig. S5(b)†). Further increasing the amount of Ce^{3+} to 0.15 mmol (sample 9) resulted in the disappearance of the nanoparticles and the obtained hierarchical superstructures possess more complex structure (Fig. S5(c)†). Well-defined Ce-CP hierarchical superstructures were obtained at 0.2 mmol Ce^{3+} (sample 1). On the basis of the above results, we would like to point out that the concentration of reactants also plays a crucial role in determining the morphology of the products, and a high concentration of reactants favors the formation of pure and high yield Ce-CP hierarchical superstructures in a definite reaction time, and the typical Ce-CP hierarchical superstructures could be selectively obtained at high concentration of reactants (sample 1).

It was found that the solvent composition also had great effect on the morphology of the final product. Considering that the poor solubility of 2,5-H_2pdc in ethanol, pure ethanol as the solvent could not carry out in this experiment. When 12 mL of dmf and 20 mL of ethanol was used as the solvent media (sample 10), the product was mainly composed of typical hierarchical superstructures and some detached branches were also found in the product (Fig. S6(a)†). When the solvent was composed of 22 mL of dmf and 10 mL of ethanol (sample 1), well-defined Ce-CP hierarchical superstructures were obtained on a large scale (Fig. 1). No hierarchical superstructures were observable and only uniform spheres with diameters of about 1 μm were obtained (Fig. S6(b)†) when pure dmf was used as the solvent (sample 11). The results further confirm that the composition of solvent is also an important factor to control morphology evolution of the as-prepared products.
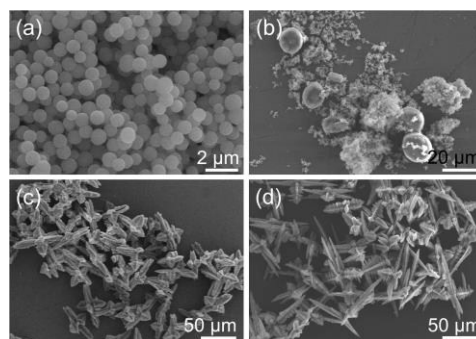

Fig. 2 SEM images of the products obtained at 160 ^{o}C with different times of (a) 1 h (sample 12), (b) 80 min (sample 13), (c) 1.5 h (sample 14), and (d) 24 h (sample 15), respectively.

In addition, time-dependent experiments were also conducted in this work. When the reaction time was 1 h (sample 12), a large quantity of uniform nanospheres with the diameters of about 500 nm were obtained (Fig. 2(a)). After 80 min (sample 13) of reaction, the nanospheres began to agglomerate and produce microstructured spheroids of about 20 μm in diameter (Fig. 2(b)). At the same time, some nanospheres adhering to the surface of spheroid could be found, which proved that these spheroids particles were composed of nanospheres. When the reaction time was prolonged to 1.5 h (sample 14), the product was mainly composed of poor-formed hierarchical superstructures, representing the 3D hierarchical superstructure gradually extended (Fig. 2(c)). Extending the reaction time to 12 h (sample 1), hierarchical superstructures with the length of dendritic structures of 10-50 μm self-assembled by nanoparticles were obtained (Fig. 1). After further prolonging the reaction time to 24 h (sample 15), the obtained hierarchical superstructures became more complex and possessed a broad size distribution (Fig. 2(d)). These images clearly reveal that the Ce-CP hierarchical superstructures are composed of nanospheres and size of the Ce-CP hierarchical superstructures increases with extending the reaction time.

Possible formation mechanism of the Ce-CP hierarchical superstructures

In order to explore the formation mechanism, we examined thoroughly the as-prepared products prepared at different reaction time ranging from 60 min to 12 h while keeping other reaction

conditions the same by XRD (Fig. S7†). It can be clearly seen that the peak intensity increases with increasing reaction time. After reaction for 80 min, the XRD patterns become much stronger and narrower, indicating that the amorphous aggregates
5 have been transformed into crystalline solids, which are basically in agreement with the observation in SEM images.
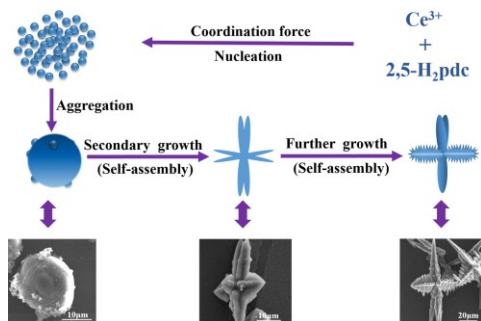
Scheme 1 Schematic illustration of the formation of the Ce-CP hierarchical superstructures.

10 The generation of branched or dendritic structures is always the result of kinetically and/or thermodynamically controlling the original nucleating stage and succeeding crystal growth stage through changing the reaction parameters.[44] Although the exact mechanism of the assembled hierarchical structure is unclear, on
15 the basis of the SEM observation, we consider that the formation of the porous Ce-CP hierarchical superstructures can be simply described as a self-assembly growth mechanism.[7b,18] A possible formation mechanism is illustrated in Scheme 1. At first, the Ce^{3+} reacts with 2,5-H_2pdc to produce primary nanospheres driven by
20 the coordination force. Subsequently, the newly formed nanospheres grow up and aggregate into microstructured spheroids driven by the minimization of interfacial energy. Furthermore, with continues growth, the freshly formed spheroids are not stable, they transform into multiple dendritic structures
25 through a self-assembly process. Finally, the hierarchical superstructures were obtained via the further self-assembly process under mixed-solvothermal treatment.

Crystal phase, morphology and properties of the as-obtained CeO_2
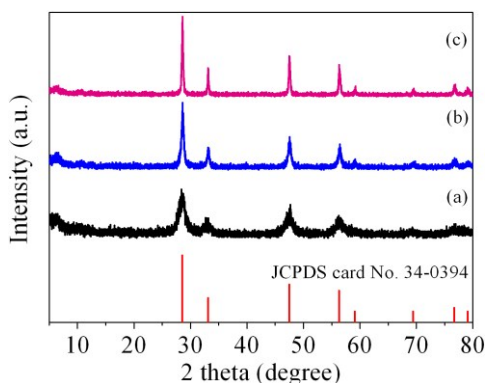

30
Fig. 3 XRD patterns of the Ce-CP hierarchical superstructures heat-treated at (a) 450 °C, (b) 500 °C, (c) 600 °C for 4 h with a heating rate of 0.5 °C min^{-1}, and the reference data of JCPDS card No. 34-0394 for pure CeO_2.

35 It has been demonstrated that micro/nano structured CP could be used as the precursors for the preparation of the corresponding metal oxides since their organic components of the coordination

polymers are readily removed by thermal decomposition.[39,45] Fig. 3 is the XRD patterns of the Ce-CP hierarchical superstructures
40 heat-treated at a temperature of 450-600 °C. The diffraction patterns exhibit the samples crystallized in face-centered cubic pure phase (space group: $Fm3m$(225)) of CeO_2 (JCPDS card No. 34-0394). No signals of impurities are detected, implying that the Ce-CP have been decomposed into CeO_2 completely. In addition,
45 it can be seen that the intensity of diffraction peak increases and half width of diffraction peak decreases with heat-treated temperature, which indicates that the crystallite size of CeO_2 grain increases with the heat-treated temperature. Furthermore, the broadening of the peaks indicates that the as-obtained CeO_2
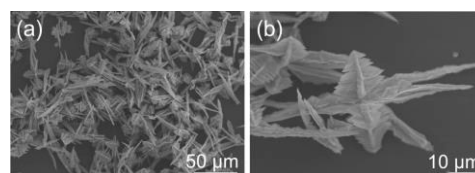50 hierarchical structures are composed of primary small crystal particles.[32]

Fig. 4 SEM images of the as-obtained CeO_2 after thermal decomposition of the Ce-CP hierarchical superstructures in air at 450 °C for 4 h.
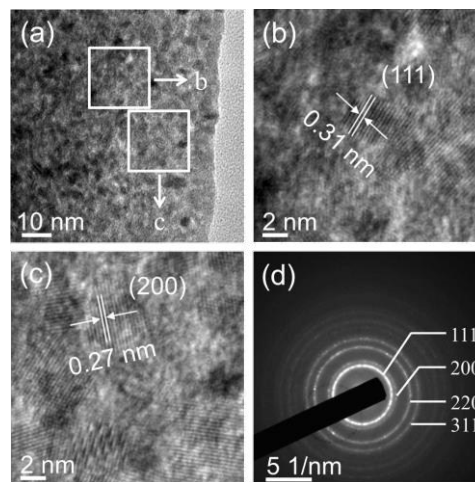

55
Fig. 5 (a-c) HRTEM images and (d) Selected-area electron diffraction (SAED) pattern of the as-obtained CeO_2.
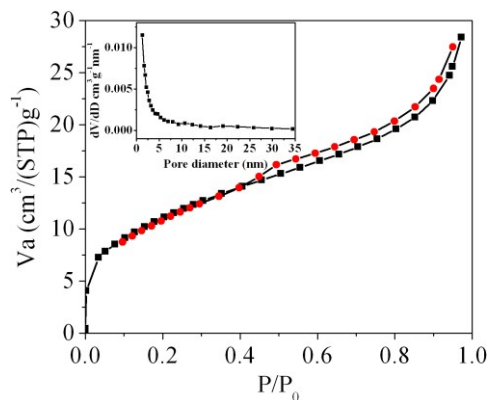

60
Fig.6 N_2 adsorption-desorption isotherms of the as-obtained CeO_2; inset is the corresponding BJH pore size distribution curve.

The morphology and architectures of the as-obtained CeO_2 were investigated by SEM and HTEM. As shown in Fig. 4(a), SEM image reveals that most of the products inherit the

morphology of its precursor. In comparison to precursor, the length shrinkage and rough surface for CeO_2 (Fig. 4(b)) may be caused by the escape of H_2O and gas molecules from the surface during the thermal decomposition-oxidation to CeO_2 process.

[5] HRTEM image (Fig. 5a-c) clearly shows that the CeO_2 consists of quantities of ceria nanocrystals which pack together in different directions to form the mesopores (Fig. 5a), and this is confirmed by N_2 adsorption-desorption isotherms (discuss later). The lattice fringes are clearly visible with a spacing of 0.31 nm

[10] and 0.27 nm, corresponding to the spacing of the (111) and (200) planes of cubic ceria. The SAED ring pattern (Fig. 5d) further indicates that the structure of the obtained product is a face-centered cubic CeO_2. The N_2 adsorption-desorption isotherms (Fig. 6) were used to characterize the porosity of the as-obtained

[15] CeO_2 after pretreatment at 150 °C for 4 h under vacuum conditions. It is found that the CeO_2 exhibits typical IV characteristics with an obvious hysteresis loop, suggesting that there are mesopores in CeO_2.[46] The specific surface area of CeO_2 calculated by the Brunauer-Emmett-Teller (BET) method is 35.90

[20] $m^2 g^{-1}$, which is higher than that of commercial CeO_2 powder (a surface area of *ca.* 10.23 $m^2 g^{-1}$). The pore size distribution was calculated from the adsorption branch through the Barett-Joyner-Halenda (BJH) method and shown in the inset of Fig. 6, which indicates that the pore distribution is in a wide range and the

[25] average pore diameter of the CeO_2 is about 4.89 nm.[45a] Furthermore, no diffraction peaks could be observed in the small-angle XRD pattern of the as-prepared CeO_2 (Fig. S8†), suggesting that the mesoporous are not periodically organized, which is in good accordance with the aforementioned HRTEM

[30] images. The Raman spectra of the as-obtained CeO_2 under ambient conditions are shown in Fig. S9†. The 464 cm^{-1} band is attributed to the Raman-active symmetry vibrational mode (F_{2g}) of CeO_2 fluorite-type structure, a weak band between 540 cm^{-1} and 600 cm^{-1} could prove the existence of oxygen vacancies.[47]
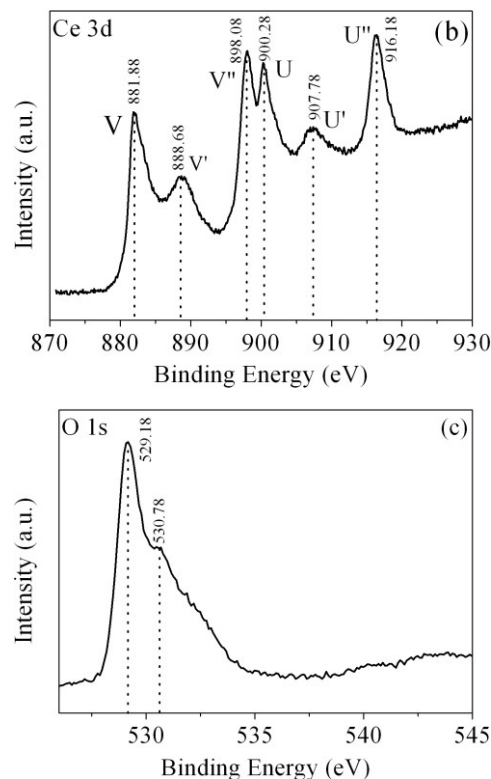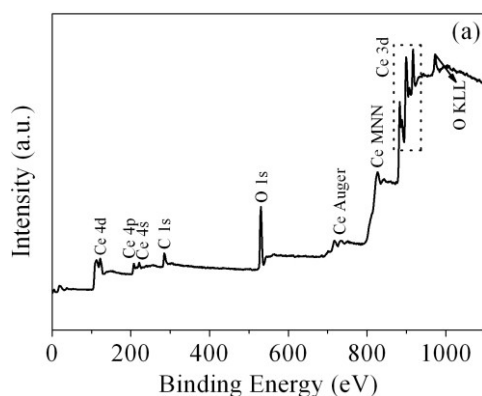

Fig. 7 (a) XPS wide-survey spectrum, (b) Ce 3d core level XPS spectrum and (c) O 1s core level XPS spectrum of the as-obtained CeO_2.

[40] To further characterize the product, XPS were conducted to further investigate the surface composition and chemical state of the as-obtained CeO_2. The wide-survey XPS spectrum of the as-obtained CeO_2 (Fig. 7(a)) reveals the predominant presence of Ce, O signals on the surface of the sample, which indicates the

[45] high purity of the as-obtained CeO_2 sample. The minor amount of carbon element with binding energy at 285.98 eV arises from the adventitious carbon. Fig. 7(b) displays the Ce 3d core level XPS spectrum of the as-obtained CeO_2, which consists of two series of V and U peaks corresponding to $3d_{5/2}$ and $3d_{3/2}$ states,

[50] respectively, consistent with the previous report of Ce^{4+} states. For $3d_{5/2}$ of Ce(IV), the peaks of V and V' can be attributed to a mixing of the $3d^9 4f^2(O2p^4)$ and $3d^9 4f^1(O2p^5)Ce^{4+}$ states, and V'' to the $3d^9 4f^0(O2p^6)Ce^{4+}$ state. The origin of the U structures, due to the Ce $3d_{3/2}$ level, can be carried out in the same way.[48] It is

[55] clearly that the valley between V and V' is assigned to $3d^9 4f^1(O2p^6)Ce^{3+}$ final state, which indicates that a small quantity of Ce^{3+} is also present in the sample.[28] One can determine the relative amount of Ce^{3+} from the relative peak areas of Ce^{3+}/total areas ratio.[49] However, it is difficult to obtain a definite value due

[60] to the complex backgrounds. Fig. 7(c) shows the O 1s core level XPS spectrum of the as-obtained CeO_2, which can be deconvolved into two peaks. The peak at 530.78 eV could be assigned to the absorbed oxygen, and another peak located at a lower BE (529.18 eV) originated from the lattice oxygen.[50]
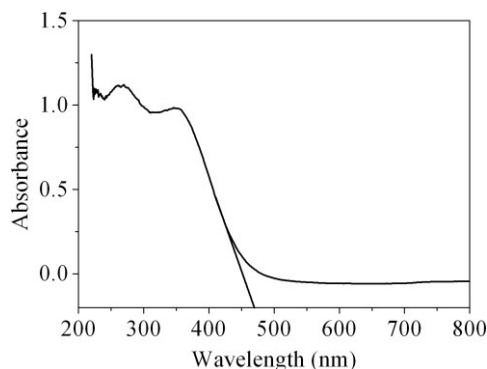
Fig. 8 Uv-vis spectrum of the as-obtained CeO_2.

As is well known, CeO_2 can be used as a nice ultraviolet-blocking material arising from the charge transfer transitions
[5] from O^{2-} in O 2p to Ce^{4+} in Ce 4f state. The UV-vis absorption spectrum of the obtained CeO_2 sample is shown in Fig. 8. As we can see from the spectrum, the CeO_2 sample has a strong absorption in the UV region. The optical band gap Eg can be calculated based on the following equation: $Eg = 1240/\lambda_{AE}$, where
[10] λ_{AE} represents the edge wavelength of absorbance. The onset of absorption for our prepared CeO_2 is at 469 nm, corresponding to the band gap energy (Eg) of 2.64 eV, which is fairly lower than that of bulk ceria (Eg = 2.82 eV). In general, reducing in crystalline size would lead to the increase of the band gap width
[15] owing to the quantum size effect.[51] However, our work is not in agreement with this viewpoint, and similar result has also been observed in 3D hierarchical flowerlike CeO_2 microspheres reported by Lu and co-workers.[52] There are two plausible theories for the expatiation of the final moderato red-shift of the CeO_2.
[20] The existence of quantum confinement effect due to the nanoscale size of the primary particles forming the mesoporous CeO_2 with hierarchical structures resulted in a red-shift in the UV-vis spectrum.[53] On the other hand, ceria possesses intrinsic defect (Ce^{3+} and O vacancy concentration) in the fluorite
[25] structure, which generally introduces intermediate energy levels, resulting in a decrease in the band gap. Therefore, it can be speculated that a decrease in band gap for sample indicates there has been more Ce^{3+} and O vacancy concentration in mesoporous CeO_2.[52]
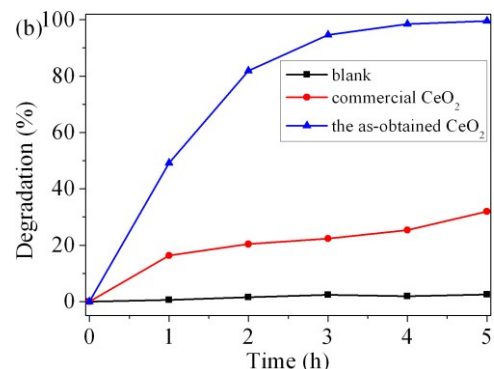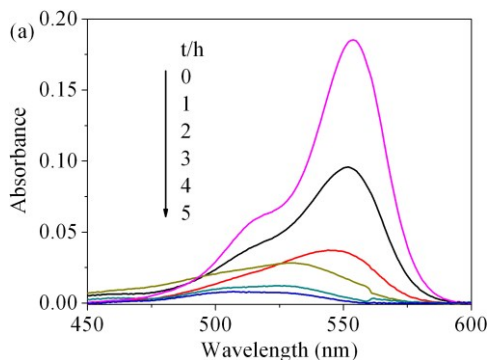

[30]

Fig. 9 (a) Temporal Uv-vis spectroscopic changes of the RhB aqueous solution in the presence of the as-obtained CeO_2 under exposure to UV light, (b) Degradation rate of RhB in the dark under UV light: (blue line)
[35] the as-obtained CeO_2, (red line) commercial CeO_2, and (black line) without a photocatalyst.

To evaluate the photocatalytic activity of the as-obtained CeO_2, the photodegradation of RhB was carried out. Fig. 9(a) shows the visible spectral changes during the photocatalytic degradation of
[40] RhB in the presence of CeO_2 under UV light irradiation. The characteristic absorption of RhB at 554 nm was used to monitor the degradation process as a function of irradiation time. The change of the absorption of RhB aqueous solution represented the change in the concentration. It can be seen that the characteristic
[45] adsorption peak of RhB diminished quickly with the increase of irradiation time in the degradation process and almost disappeared after 5 h. The degradation rate (%) of RhB is defined as $(C_0 - C)/C_0 \times 100\%$, where C and C_0 represent the remnant and initial concentration of RhB, respectively. Fig. 9(b) displays
[50] the degradation rate of RhB on the two catalysts under UV light irradiation as well as the results of blank tests. After 5 h of illumination, compared to the blank experiment without photocatalyst, the addition of CeO_2 catalysts obviously promoted the degradation of RhB. The photocatalytic degradation rate of
[55] RhB solution for as-obtained CeO_2 reaches 99.6%, while the commercial CeO_2 powder is only 32.0%. These results suggest that the as-obtained CeO_2 exhibits good photocatalytic activity. The superior photocatalytic performances of CeO_2 can be attributed to two factors. One is that the as-obtained mesoporous
[60] CeO_2 possess higher surface areas and facilitate the adsorption of the RhB molecules, which would greatly improve the catalytic efficiency.[18] The other is assigned to the oxygen vacancies on the surface of mesoporous CeO_2, as revealed by XPS analysis mentioned above. These abundant surface oxygen vacancies can
[65] bear a negative charge, and thus they can conveniently combine with the cationic groups of RhB via strong electrostatic attraction to form V_o-$^+$N (V_o, oxygen vacancy; $^+$N, the charged N in RhB) as well as hydrogen bonding with the nitrogen atoms of RhB.[54]

Conclusions

[70] In summary, we have successfully synthesized Ce-CP hierarchical superstructures by a simple one-pot mixed-solvothermal method without any additional template or surfactant. The results demonstrated that it is possible to control the size and morphology of the Ce-CP hierarchical
[75] superstructures by adjusting process parameters such as reaction

temperature, reaction time, total concentrations, and solvent composition of the reactants. A possible growth mechanism called self-assembly has been proposed to explain the formation of the Ce-CP hierarchical superstructures, as shown by SEM and XRD investigations. Besides, CeO_2 with similar hierarchical structures were successfully synthesized by thermal conversion of the Ce-CP in air at 450 ^{o}C for 4 h. In addition, the as-obtained CeO_2 exhibit high activity towards the photocatalytic degradation for organic pollutants (RhB) under high-pressure mercury lamp. Thus, the as-obtained mesoporous CeO_2 products may have potential application in elimination organic pollutants in wastewater.

Acknowledgements

Notes and references

1 J. M. Amigo, T. Skov and R. Bro, *Chem. Rev.*, 2010, **110**, 4582-4605.

2 M. P. Suh, H. J. Park, T. K. Prasad and D.-W. Lim, *Chem. Rev.*, 2012, **112**, 782-835.

3 D. Liu, R. C. Huxford and W. Lin, *Angew. Chem., Int. Ed.*, 2011, **50**, 3696-3700.

4 F. Ke, Y.-P. Yuan, L.-G. Qiu, Y.-H. Shen, A.-J. Xie, J.-F. Zhu, X.-Y. Tian and L.-D. Zhang, *J. Mater. Chem.*, 2011, **21**, 3843-3848.

5 J. Huo, L. Wang, E. Irran, H. Yu, J. Gao, D. Fan, B. Li, J. Wang, W. Ding, A. M. Amin, C. Li and L. Ma, *Angew. Chem., Int. Edit.*, 2010, **49**, 9237-9241.

6 S. Jung, W. Cho, H. J. Lee and M. Oh, *Angew. Chem., Int. Edit.*, 2009, **48**, 1459-1462.

7 (a) S.-L. Zhong, R. Xu, L.-F. Zhang, W.-G. Qu, G.-Q. Gao, X.-L. Wu and A.-W. Xu, *J. Mater. Chem.*, 2011, **21**, 16574-16580; (b) S. Zhong, M. Wang, L. Wang, Y. Li, H. M. Noh and J. H. Jeong, *CrystEngComm*, 2014, **16**, 231-236; (c) D. Zhao, L. Wang, Y. Li, L. Zhang, Y. Lv and S. Zhong, *Inorg. Chem. Commun.*, 2012, **20**, 97-100; (d) L. Luo, R. Xu, D. Zhao and S. Zhong, J. *Rare Earths*, 2010, **28**, 106-110; (e) L. Wang, D. Zhao, S.-L. Zhong and A.-W. Xu, *CrystEngComm*, 2012, **14**, 6875-6880; (f) S. Zhong, H. Jing, Y. Li, S. Yin, C. Zeng and L. Wang, *Inorg. Chem.*, 2014, **53**, 8278-8286.

8 (a) W. Lin, W. J. Rieter and K. M. L. Taylor, *Angew. Chem., Int. Edit.*, 2009, **48**, 650-658; (b) W. Cho, H. J. Lee and M. Oh, *J. Am. Chem. Soc.*, 2008, **130**, 16943-16946; (c) F.-X. Bu, M. Hu, L. Xu, Q. Meng, G.-Y. Mao, D.-M. Jiang and J.-S. Jiang, *Chem. Commun.*, 2014, **50**, 8543-8546; (d) S. Jung and M. Oh, *Angew. Chem., Int. Edit.*, 2008, **47**, 2049-2051.

9 (a) B. Lim and Y. Xia, *Angew. Chem., Int. Edit.*, 2011, **50**, 76-85; (b) V. Polshettiwar, M. N. Nadagouda and R. S. Varma, *Chem. Commun.*, 2008, 6318-6320; (c) M. Cao, T. Liu, S. Gao, G. Sun, X. Wu, C. Hu and Z. L. Wang, *Angew. Chem., Int. Edit.*, 2005, **44**, 4197-4201.

10 J. Zhang, Q. Xu, Z. Feng, M. Li and C. Li, *Angew. Chem., Int. Edit.*, 2008, **47**, 1766-1769.

11 I. Lisiecki, P.-A. Albouy and M.-P. Pileni, *Adv. Mater.*, 2003, **15**, 712-716.

12 S. Bharathi, D. Nataraj, M. Seetha, D. Mangalaraj, N. Ponpandian, Y. Masuda, K. Senthil and K. Yong, *CrystEngComm*, 2010, **12**, 373-382.

13 Z. Jiang, Z. Li, Z. Qin, H. Sun, X. Jiao and D. Chen, *Nanoscale*, 2013, **5**, 11770-11775.

14 M. Chen, Y. N. Kim, C. Li and S. O. Cho, *Cryst. Growth Des.*, 2008, **8**, 629-634.

15 P. Chen, L. Gu and X. Cao, *CrystEngComm*, 2010, **12**, 3950-3958.

16 Z. Yu, Z. Yao, N. Zhang, Z. Wang, C. Li, X. Han, X. Wu and Z. Jiang, *J. Mater. Chem. A*, 2013, **1**, 4571-4576.

17 G. Shen, D. Chen and C. J. Lee, *J. Phys. Chem. B*, 2006, **110**, 15689-15693.

18 L.-P. Zhu, N.-C. Bing, L.-L. Wang, H.-Y. Jin, G.-H. Liao and L.-J. Wang, *Dalton Trans.*, 2012, **41**, 2959-2965.

19 H.-J. Kim, K.-I. Choi, A. Pan, I.-D. Kim, H.-R. Kim, K.-M. Kim, C. W. Na, G. Cao and J.-H. Lee, *J. Mater. Chem.*, 2011, **21**, 6549-6555.

20 S. Z. Li, H. Zhang, J. B. Wu, X. Y. Ma and D. R. Yang, *Cryst. Growth Des.*, 2006, **6**, 351-353.

21 K. Liu, H. You, G. Jia, Y. Zheng, Y. Huang, Y. Song, M. Yang, L. Zhang and H. Zhang, *Cryst. Growth Des.*, 2010, **10**, 790-797.

22 S. Carrettin, P. Concepción, A. Corma, J. M. L. Nieto and V. F. Puntes, *Angew. Chem., Int. Edit.*, 2004, **43**, 2538-2540.

23 B. P. Pearman, N. Mohajeri, R. P. Brooker, M. P. Rodgers, D. K. Slattery, M. D. Hampton, D. A. Cullen and S. Seal, *J. Power Sources*, 2013, **225**, 75-83.

24 X. Jiao, H. Song, H. Zhao, W. Bai, L. Zhang and Y. Lv, *Anal. Methods*, 2012, **4**, 3261-3267.

25 N. Izu, T. Uchida, I. Matsubara, T. Itoh, W. Shin and M. Nishibori, *Mater. Res. Bull.*, 2011, **46**, 1168-1176.

26 (a) D. Zhang, X. Du, L. Shi and R. Gao, *Dalton Trans.*, 2012, **41**, 14455-14475; (b) D. Zhang, F. Niu, T. Yan, L. Shi, X. Du and J. Fang, *Appl. Surf. Sci.*, 2011, **257**, 10161-10167; (c) J. Zhang, S. Ohara, M. Umetsu, T. Naka, Y. Hatakeyama and T. Adschiri, *Adv. Mater.*, 2007, **19**, 203-206; (d) L. Wang, L.-F. Zhang, S.-L. Zhong and A.-W. Xu, *Appl. Surf. Sci.*, 2012, **263**, 769-776.

27 H. Mai, D. Zhang, L. Shi, T. Yan and H. Li, *Appl. Surf. Sci.*, 2011, **257**, 7551-7559.

28 Z. Sun, H. Zhang, G. An, G. Yang and Z. Liu, *J. Mater. Chem.*, 2010, **20**, 1947-1952.

29 S. Yang and L. Gao, *J. Am. Chem. Soc.*, 2006, **128**, 9330-9331.

30 Z. Ji, X. Wang, H. Zhang, S. Lin, H. Meng, B. Sun, S. George, T. Xia, A. E. Nel and J. I. Zink, *Acs Nano*, 2012, **6**, 5366-5380.

31 L.-S. Zhong, J.-S. Hu, A.-M. Cao, Q. Liu, W.-G. Song and L.-J. Wan, *Chem. Mater.*, 2007, **19**, 1648-1655.

32 W. Liu, L. Feng, C. Zhang, H. Yang, J. Guo, X. Liu, X. Zhang and Y. Yang, *J. Mater. Chem. A*, 2013, **1**, 6942-6948.

33 M. Eddaoudi, H. Li and O. M. Yaghi, *J. Am. Chem. Soc.*, 2000, **122**, 1391-1397.

34 A. Querejeta- Fernández, J. C. Hernández-Garrido, H. Yang, Y. Zhou, A. Varela, M. Parras, J. J. Calvino- Gámez, J. M. González-Calbet, P. F. Green and N. A. Kotov, *Acs Nano*, 2012, **6**, 3800-3812.

35 Z. Shen, S. He, P. Yao, X. Lao, B. Yang, Y. Dai, X. Sun and T. Chen, *Rsc Adv.*, 2014, **4**, 12844-12848.

36 R. Kaminker, R. Popovitz-Biro and M. E. van der Boom, *Angew. Chem., Int. Edit.*, 2011, **50**, 3224-3226.

37 K. Liu, H. Liu, L.-L. Yang, F.-Y. Zhao, Y. Li and W.-J. Ruan, *RSC Adv.*, 2014, **4**, 25160-25164.

38 H. Qiao, Y. Jia, Y. Zheng, N. Guo, Q. Zhao, W. Lv and H. You, *CrystEngComm*, 2012, **14**, 5830-5835.

39 Y. Zheng, K. Liu, H. Qiao, Y. Zhang, Y. Song, M. Yang, Y. Huang, N. Guo, Y. Jia and H. You, *CrystEngComm*, 2011, **13**, 1786-1788.

40 P. Silva, A. A. Valente, J. Rocha and F. A. A. Paz, *Cryst. Growth Des.*, 2010, **10**, 2025-2028.

41 V. I. Isaeva, E. V. Belyaeva, A. N. Fitch, V. V. Chernyshev, S. N. Klyamkin and L. M. Kustov, *Cryst. Growth Des.*, 2013, **13**, 5305-5315.

42 W. Steele, *Chem. Rev.*, 1993, **93**, 2355-2378.

43 C. Li, J. Yang, P. Yang, H. Lian and J. Lin, *Chem. Mater.*, 2008, **20**, 4317-4326.

44 L.-W. Qian, X. Wang and H.-G. Zheng, *Cryst. Growth Des.*, 2012, **12**, 271-280.

45 (a) Z. Shen, J. Liu, F. Hu, S. Liu, N. Cao, Y. Sui, Q. Zeng and Y. Shen, *CrystEngComm*, 2014, **16**, 3387-3394; (b) Z. Sharifzadeh,

S. Abedi and A. Morsali, *J. Mater. Chem. A*, 2014, **2**, 4803-4810; (c) Y. Lu, H. Cao, S. Zhang and X. Zhang, *J. Mater. Chem.*, 2011, **21**, 8633-8639; (d) H.-Y. Shi, B. Deng, S.-L. Zhong, L. Wang and A.-W. Xu, *J. Mater. Chem.*, 2011, **21**, 12309-12315; (e) M. Wang, F. Wang, J. Ma and J. Xu, *J. Mater. Chem. A*, 2014, **2**, 15480-15487.

46 G. Zhang, Z. Shen, M. Liu, C. Guo, P. Sun, Z. Yuan, B. Li, D. Ding and T. Chen, *J. Phys. Chem. B*, 2006, **110**, 25782-25790.

47 M. Guo, J. Lu, Y. Wu, Y. Wang and M. Luo, *Langmuir*, 2011, **27**, 3872-3877.

48 P. Ji, J. Zhang, F. Chen and M. Anpo, *J. Phys. Chem. C*, 2008, **112**, 17809-17813.

49 H. Borchert, Y. V. Frolova, V. V. Kaichev, I. P. Prosvirin, G. M. Alikina, A. I. Lukashevich, V. I. Zaikovskii, E. M. Moroz, S. N. Trukhan, V. P. Ivanov, E. A. Paukshtis, V. I. Bukhtiyarov and V. A. Sadykov, *J. Phys. Chem. B*, 2005, **109**, 5728-5738.

50 H.-I. Chen and H.-Y. Chang, *Solid State Commun.*, 2005, **133**, 593-598.

51 N. K. Renuka, *J. Alloys Compd.*, 2012, **513**, 230-235.

52 J. Li, G. Lu, H. Li, Y. Wang, Y. Guo and Y. Guo, *J. Colloid Interface Sci.*, 2011, **360**, 93-99.

53 S. Yuan, Q. Zhang, B. Xu, Z. Jin, Y. Zhang, Y. Yang, M. Zhang and T. Ohno, *RSC Adv.*, 2014, **4**, 62255-62261.

54 H. Xiao, Z. Ai and L. Zhang, *J. Phys. Chem. C* 2009, **113**, 16625–16630.

Table of content
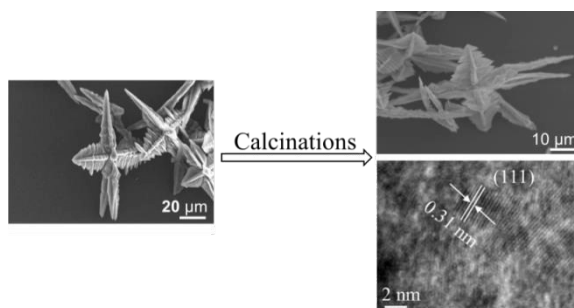
Novel three-dimensional (3D) ceria hierarchical structures have been prepared via a thermolysis of the corresponding porous coordination polymer precursors.